Near-Field Antenna Measurements using a Lithium Niobate Photonic Probe

Vince Rodriguez[1], Brett Walkenhorst[1], and Jim Toney[2]
[1]NSI-MI Technologies, Suwanee, Georgia, USA, Vrodriguez@nsi-mi.com
[2]Srico, Columbus, Ohio USA

***Abstract*—Recently, a paper was presented in which a lithium niobate ($LiNbO_3$) crystal electric field sensor was characterized as a possible probe for near-field antenna measurements. In the present paper, some preliminary measurements are presented. A standard gain horn operating in the X-band was measured in a spherical near-field range using the $LiNbO_3$ probe as the near-field probe. The results are compared to computed data for said horn. An additional flat-plate, slotted array antenna operating in the X-band was also measured. The data was transformed to the far field and compared with previous measurements of said antenna performed using a traditional open-ended-waveguide (OEWG) probe. Additionally, the transform was used to back-project to the aperture of the antenna and the data show the two slots in the array that are covered with metallic tape. The transforms and back-projection suggest that these probes could be used as near-field probes in antenna measurements if some stability issues are corrected.**

***Index Terms*—Antenna Measurements, Photonic Probes.**

I. Introduction

The possibility of using photonic electric-field probes was presented recently [1]. These photonic sensors use a lithium niobate Mach-Zehnder interferometer (MZI) to sense the electric field. A laser that propagates via fiber-optic cable is modulated by the electric field incident on the crystal. An optical receiver is then used to extract the amplitude and phase of the electric field incident on the crystal. One of the advantages of these sensors is their extremely wide frequency bandwidth ranging from as low as 1 Hz to as high as 20 GHz. The actual usable bandwidth of a single near-field probe may be somewhat smaller, depending on the specific device geometry. In [1], it was shown that a photonic probe exhibits a cross-polarization that degrades from -45 dB to -27 dB across the Ku-band. The same probe, however, exhibits better than -35 dB of cross polarization from 1.7 GHz to 12.4 GHz. The other concern for these probes is their gain. As reported in [1], the gain is about 40 to 30dB lower than an open-ended waveguide (OEWG) probe. Another limitation is the fact that these are receive-only probes. The preliminary receive patterns for the probes presented in [1] showed a very broad beam pattern that could potentially simplify transformations since there may be no need for probe correction. The primary challenge of the MZI is the tendency of the operating point to drift with environmental fluctuations, causing instability in the sensor response. Stabilization of the sensor response is crucial in applications that involve data acquisition over an extended time or over a wide range of operating temperatures [2]. In this paper, the probe characterized in [1] is used to measure two antennas in the near-field in a spherical near-field (SNF) range.

II. Measurement of a Standard Gain Horn (SGH)

An X-band SGH was measured. The horn is a model MI-212-8.2 with a nominal gain of 22.1 dBi. It was measured in the spherical near-field chamber at the NSI-MI Technologies facility in Suwanee, Georgia. This range is a fully anechoic room that is 4.57m wide by 4.57 m tall and 6.1 m long. The range is lined with 0.26 m thick pyramidal absorber on the side walls and ceiling. The floor between the antenna under test (AUT) and the field probe is covered by 0.61 m tall pyramidal absorber. The end wall behind the probe is covered by 0.61 m thick pyramidal absorber. The end wall behind the AUT is covered with 0.26 m pyramidal absorber.

The minimum sphere was set to 1.52 m in diameter with the probe sampling right on the edge of the sphere. The data for a hemisphere was transformed to the far field. The resultant pattern is shown in Figure 1 for 8.2 GHz. The directivity of the pattern is very close to the expected values. The computed pattern has a directivity of 21.5 dBi and the measured pattern shows a directivity of 21.2 dBi. Hence the directivities were within 0.3 dB of each other. It should be noted that the 22.1 dBi nominal gain value is for the center of the band. A lower directivity and gain is expected at the low end of the band.

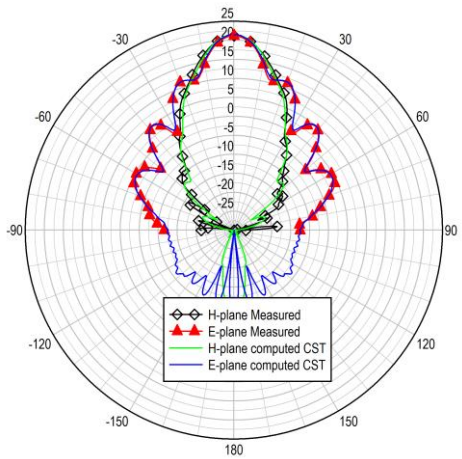

Figure 1. Pattern for the two principal planes at ?? GHz. The measured data is transformed from -90° to 90°

The normalized pattern data for 8.2 GHz and 12.4 GHz is shown in more detail in Figure 2 and in Figure 3. The comparison at 8.2 GHz looks very promising. The half power beamwidths for each plane are summarized in TABLE I.

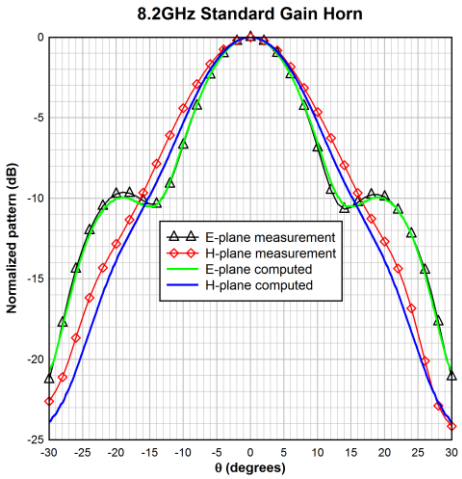

Figure 2. Comparison of measured and computed data for a standard gain horn at 8.2 GHz.

TABLE I. HPBW COMPARISON FOR SGH AT 8.2GHZ

Principal plane	*Measured HPBW*	*Computed HPBW*	*% difference*
E-plane	13.58°	13.58°	0.%
H-plane	15.92°	14.73°	8.07%

The sidelobes on the E-plane appear at the same angle and the sidelobe levels (SLL) appear to be the same in both the computed and the measured data sets.

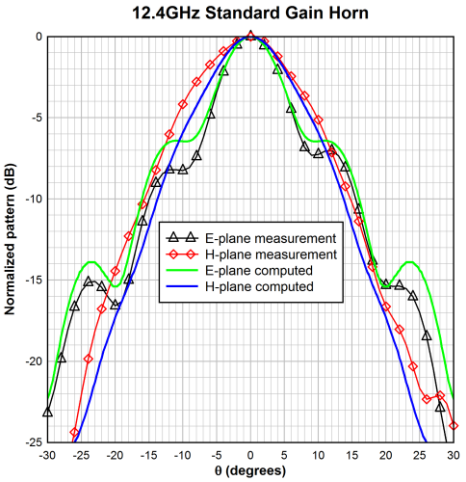

Figure 3. Comparison of measured and computed data for a SGH at 12.4 GHz.

However, as the frequency increases and the data is compared at 12.4 GHz, more variation is seen between the computed and measured patterns. The HPBW exhibits errors of up to 20.5% on the H-plane as seen in TABLE II. The SLLs have differences of up to 1.75 dB.

TABLE II. HPBW COMPARISON FOR SGH AT 12.4 GHZ

Principal plane	*Measured HPBW*	*Computed HPBW*	*% difference*
E-plane	9.48°	9.75°	-2.78%
H-plane	15.28°	12.68°	-20.5%

The measured directivity of the horn at 12.4 GHz was 22.63 dBi. The computed directivity per CST was 22.81 dBi; hence the difference in directivity was only 0.18 dB, which is smaller than the difference between computed and measured at 8.2 GHz.

One could point to the range as the source of the error since the angular response of the $LiNbO_3$ probe is very broad [1] and will potentially be affected by the reflected energy from the walls. A simplified ray-tracing approach intended for rectangular anechoic chambers is used to analyze the expected reflected energy arriving to the near-field probe using the techniques and approximations presented in [4] and [5]. The analysis uses the size of the anechoic range and the approximated off-angle reflectivity of the absorber. The separation between the center of the minimum radiating sphere (MRS) in the SNF transform and the photonic probe is 0.76m, so the angles of incidence onto the absorber are 11°. As it was shown in [4], this provides a reflectivity close to the normal incidence of the pyramidal absorber. For the 0.26 m (8.5 inches) absorber, the normal incidence reflectivity per the manufacturer's specifications is equal or better than -50dB. The additional path losses compared to the direct path between the probe and the center of the MRS must be added to the reflectivity [6]. Doing so, the calculation shows that the reflected waves are about -70 dB compared to the direct path. Clearly the range has very little effect on -6 dB and -14 dB SLL. The fact that the 8.2 GHz measured patterns are a closer match to the computed than the 12.4 GHz measured patterns also supports the idea that the effects are not related to the range since the reflectivity is bound to improve with increases in frequency.

Another potential source of error is instability in the operating point of the MZI. The operating point is determined by the optical path length difference between the two optical waveguide branches of the interferometer inside the lithium niobate crystal. Small physical changes in the lengths or refractive index of these branches due to temperature fluctuations can lead to significant phase changes at optical frequencies. This can have a significant impact on the operating point and, consequently, the small-signal response of the device. Preliminary data from this measurement campaign suggests that this may be affecting the patterns presented in this paper.

Another source of error could be the truncation. For the SNF acquisition, only the front hemisphere of the MRS was measured. While it is right that beyond θ=90°, the radiated energy is lower than –36 dB compared to the peak, there is a

small potential truncation error. To check this, a much higher directivity antenna was measured.

III. Measurement of a Flat Plate Slot Array

A second antenna was measured in the same SNF range using the photonic field sensor as the near-field probe. The antenna is a flat, slotted array operating at 9.375 GHz. The antenna size is 0.457 m in diameter. Figure 4 shows a picture of the antenna mounted to the AUT positioner in the SNF range. This antenna has previously been measured using the SNF technique [7]. In addition, its pattern has also been measured in a compact range (CR) [7]. The measured patterns using these two different approaches were shown to agree down to -45 dB SLL as reported in [7].

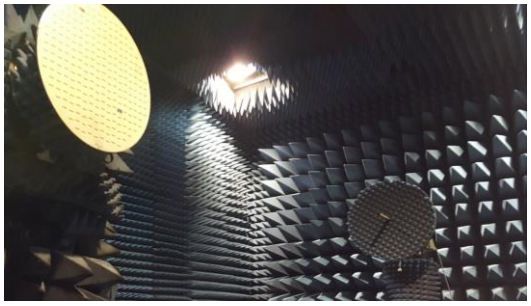

Figure 4. The flat, slotted array antenna mounted to the AUT positioner in the SNF range. Notice the two slots covered with copper tape.

The flat array antenna was measured using the photonic probe and the near- to far-field transform was applied. Initial far-field patterns were quite poor, but after looking at the near-field data at the pole, it was determined that the response of the probe likely drifted over time. As an example, Figure 5 shows the phase response for two different acquisitions at the pole for two polarizations, which were acquired one after the other.

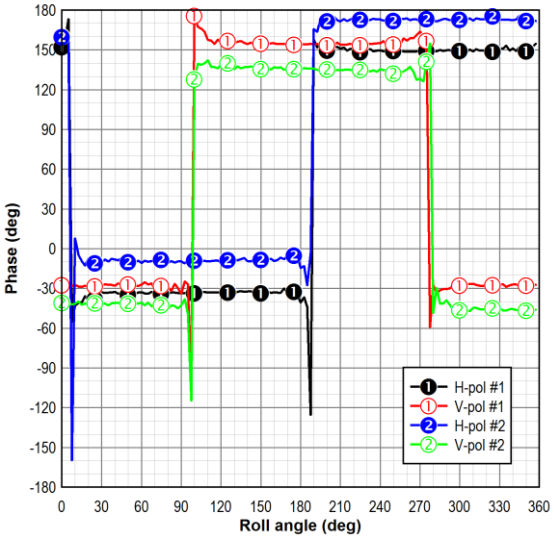

Figure 5. Phase response of polar near-field cuts for two different acquisitions and two different polarizations.

The misalignment of phase between the two polarizations suggests that the response of the probe may have drifted between the two acquisitions. Channel balancing was applied to roughly correct for the drift between acquisitions before transformation. However, nothing was done to attempt to correct for drift within a single acquisition. It is likely that results could be further improved if such a correction were applied.

Shown in Figure 6 is the far-field data compared with the compact range data presented in [7].

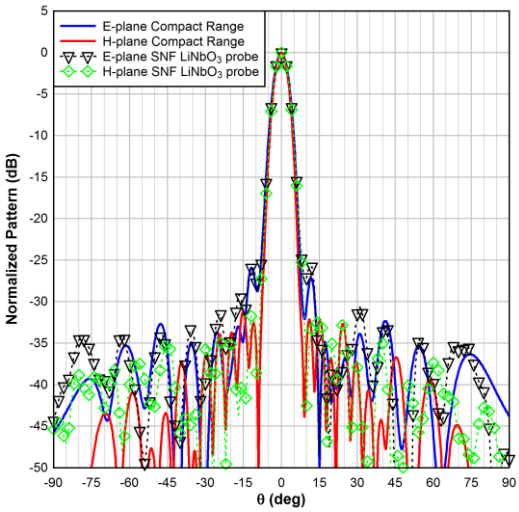

Figure 6. Comparison of the far field data obtained from the near-field data measured using the photonic probe and the compact range data reported in [7].

The data shows good agreement except for levels under -30 dB or less. In TABLE III. the HPBW is compared. There is a small difference between the two approaches.

TABLE III. HPBW comparison for SGH at 8.2GHz

Principal plane	*SNF HPBW*	*CR HPBW*	*% difference*
E-plane	5.4°	5.6°	-3.57%
H-plane	5.2°	5.1°	1.96%

A detail of the main beam and the first sidelobes is shown in **Error! Reference source not found.**. The first sidelobe on the E-plane at $\theta = -12°$ is almost a perfect match between the SNF and the CR measurements. At $\theta = 12°$ the difference is within 1.5 dB. There is a better match on the negative angles than on the positive angles. The first null and first sidelobe on the H-plane show a good match although there is a shift in the angle. The features appear shifted by about 1 degree. The second null on the H-plane of the SNF data is shifted by 1 degree and appears at $\theta = -14°$. On the other side of the peak, the second null on the E-plane completely disappears. Some of these may be related to a limit on the cross-polarization. Another source of error may be the dynamic range of the system given the low gain of the probe [1].

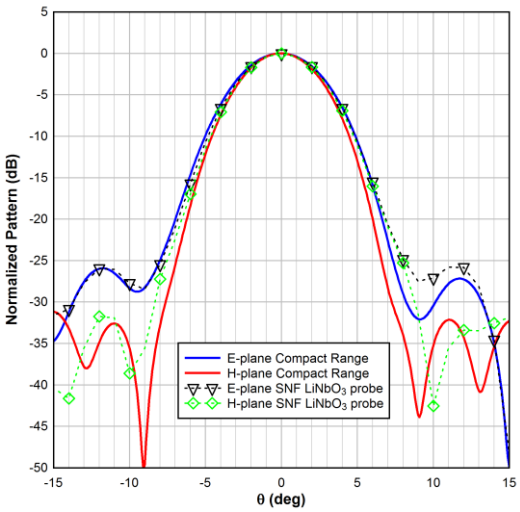

Figure 7. Detail of the main beam and first sidelobes for the measured patterns.

IV. Back Projection to the Face of the Antenna

An additional test was to perform a back projection of the field to the aperture of the antenna. In SNF measurements, the θ and ϕ components of the field are expressed as a summation of spherical modes. Once the spherical wave modes necessary to describe the measured fields on the spectral domain are found, it is possible to find the solution of the field at any location. Thus, the SNF transform allows us to back-project those fields to the surface of the AUT. Using the SNF acquisition to get the far-field pattern shown in Figure 6, the field is obtained at the aperture of the antenna. **Error! Reference source not found.** shows the back-projected fields at the aperture of the antenna.

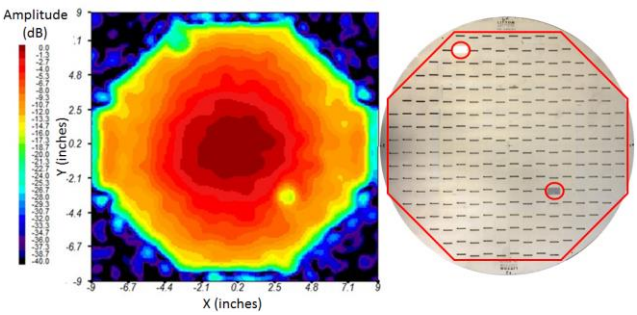

Figure 8. Field at the aperture. The antenna is shown in the figure. Notice the location of the taped slots and the disturbances of the aperture fields caused by these taped slots (dimensions are in inches).

The field distribution shows the octagonal arrangement of the slots. The antenna is also shown in **Error! Reference source not found.**. The taped slots on the array can be seen on the surface of the antenna. The field distribution shows these slots as disruptions of the field. The covered slot on the lower right sector of the octagon is clearly apparent as a region where the field drops by about 10 dB compared to the adjacent area. The slot on the upper left sector of the octagon is not as clearly defined, but it can be seen at the coordinate point (-3.25, 7.1) on the plot. The ability to get this back-projected data from the near-field data acquired using the photonic probe is very promising. It supports that this technology may be good as a near-field probe.

V. Sources of Error

While the patterns resulting from measurements made with the photonic probe are quite good, they are not ideal. Several possible sources of error have been discussed including truncation, stray signals, and operating point drift.

Truncation does not appear to be a significant factor in the patterns as two highly directive antennas were measured, both of which show some deviation from baseline patterns.

Stray signals will generally be a concern for this broadbeam probe, but in the current measurement campaign, the geometry of the antennas and the room indicate this is likely not a significant source of error.

A shift in the magnitude and phase response of the probe between successive acquisitions seems to indicate an issue with the stability of the probe's operating point. While a rough correction was performed between acquisitions, nothing was done to correct for drift within a single acquisition.

To perform such correction, several options could be employed in future work. At regular intervals, the probe could return to a single point on the near-field surface and take repeated measurements. These measurements could then be used to correct for drift over time.

Another option would be to monitor the power of the laser during the acquisition and use that information to post-process the data to correct for drift. This method has been successfully demonstrated with electrode-free z-cut sensors [3].

The operating point could be directly controlled in real-time by application of a DC bias voltage with feedback. However, the electrical cables needed to apply the voltage have the potential to perturb the electric field, obviating some of the benefits of an all-dielectric probe. An alternative that eliminates the need for an electrical cable is to apply the bias voltage by a photovoltaic power-over-fiber (POF) device. The bias control signal can then be provided by an optical fiber connection. This concept has been explored in [2]. Optimization and stabilization of the operating point have been demonstrated over a temperature range of 22°C. While initial proof-of-concept studies were done with an off-the-shelf POF module, ultimately the bare photovoltaic chip can be integrated into the sensor package to minimize perturbation of the electric field.

One final potential source of error is the lack of probe correction. Given the very dipole-like pattern of the probe as presented in [1] it was assumed that probe correction was not necessary. The need for probe correction is another point that requires further analysis.

VI. CONCLUSION

The preliminary results of antenna measurements using a $LiNbO_3$-based MZI photonic probe in near-field measurements appear very promising. In spite of potential errors such as operating point drift, the data were good enough to be able to pinpoint the taped slots on the slotted array antenna measured. In addition, most of the measured patterns agree with computed results and with measurements conducted on a CR. It should be noted that in [7] the difference between the CR and SNF using an OEWG were negligible and that there is an almost perfect match down to SLL of -45dB. While we have not achieved that level of match between results, the results do warrant further investigation to see if potential improvement to the probe such as the one described in [3] or the return-to-point check during the acquisition, can reduce the errors described in this paper. The need or not for probe correction should be investigated further as a possible source of error.

REFERENCES

[1] B. Walkenhorst, V Rodriguez, and J. Toney "Characterization of a Photonics E-Field Sensor as a Near Field Probe" 39th annual Antenna Measurement Techniques Association Symposium AMTA 2017, Atlanta, GA, October 2017.

[2] J. Toney, A. Pollick, V. Stenger, and S. Sriram, "Remote Operating Point Control of Mach Zehnder Interferometer-Based Photonic Electric Field Sensors by Power Over Fiber" 2nd International Workshop on Photonics Applied to Electromagnetic Measurements (PEM2017) Zurich, Switzerland, Octber 5-6, 2017.

[3] J.E. Toney, Lithium Niobate Photonics, pp. 192-193; Norwood, MA: Artech House; 2015.

[4] V. Rodriguez, E. Barry "A Polynomial Approximation for the Prediction of Reflected Energy from Pyramidal RF Absorbers" 38th annual Antenna Measurement Techniques Association Symposium AMTA 2016, Austin, TX, November 2016.

[5] V. Rodriguez "Validation of the Polynomial for RF Absorber Reflectivity for the Prediction of Anechoic Chambers" 2017 IEEE International Symposium on Antennas and Propagation and USNC/URSI National Radio Science Meeting, San Diego, California, July 9-14, 2017.

[6] V. Rodriguez, "Comparing Predicted Performance of Anechoic Chambers to Free Space VSWR Measurements," 39th Annual Meeting and Symposium of the Antenna Measurement Techniques Association AMTA 2017, Atlanta, GA, October 2017.

[7] J. Fordham and F. D'Agostino "Spherical Spiral Spcanning for Automotive Antenna Measurements" 37th annual Antenna Measurement Techniques Association Symposium AMTA 2015, Long Beach, CA, October 2015, pp. 143-147.